(Received 6 March 2024, Accepted 27 April 2024, Scheduled 28 November 2024)

Compact Model for EMC Analysis at Equipment Level in Automotive Context

Paul Clérico[1], Lionel Pichon[1,*], Jeffrey Lambert[2], Naraindranath Doorgah[2], and Laurent Daniel[1]

[1]*Laboratoire de Génie Electrique et Electronique de Paris, CentraleSupelec, CNRS Université Paris-Saclay, Gif-sur-Yvette 91192, France*
[2]*Forvia, Brières-les-Scellés 91150, France*

ABSTRACT: In this paper, a reconstruction methodology for the field emitted by an electronic equipment in a CISPR 25 standard environment is developed. It is based on an inverse method to determine equivalent dipoles representative of the electromagnetic sources. Positions and dipolar moments of equivalent dipoles are obtained via a hybrid optimization method, using a Genetic Algorithm (GA) followed by a Pattern Search (PS) method. First, the validity of the approach is verified with a numerical 3D model of a microstrip line. Then, an experimental protocol, corresponding to the setup of the CISPR 25 standard, is proposed and validated with a monopole antenna as a radiating source. As expected, the measurements obtained with the rod antenna yield some numerical errors related to the equivalent dipoles. However, such a compact model predicts the radiated field with sufficient accuracy to be useful for analyzing several EMC constraints in an automotive context.

1. INTRODUCTION

In recent years, one major transition in the automotive industry is the development of new technologies to reduce the consumption of fossil fuels and to attain low-emission mobility. One solution is the electrification of vehicles by integrating batteries, electric powertrains, power conversion systems, etc. However, with this increase of embedded electronic devices in such a limited place, the risk of electromagnetic interference (EMI) rises [1–4]. These interferences may affect sensitive devices, for example the on-board receiver on vehicle radio performance [5]. Thus, the radiated field of embedded electronic devices must be identified, and in some cases, its far field must be predicted. Finding simple and compact models able to predict EMI at low cost is therefore of major importance in industry.

Furthermore, in an automotive context, the emission of such devices should comply with automotive emission standards such as CISPR 25 for a large frequency range from 150 kHz to 6 GHz [6]. With the CISPR 25 test setup, the radiated field from an equipment is generally measured with a rod antenna and a biconical antenna, below and above 30 MHz, respectively. This standard ensures that the radio-frequency emissions from the equipment remain under prescribed limits. Such measurement protocol is time consuming in automotive industry but is never used to get any insight about the EMC behavior of the device under test. In [7, 8], the authors characterized radiated emissions in some specific configurations. In [7], a near-field scanning and the use of Huygens box method is used to identify the major radiating parts of a device under test or harness. In [8], a one tenth scale model approach is performed to observe the behavior of emissions from a simple transmission line source placed first on a test bench and later in a vehicle. The work focused on how the behaviour of a single wire transmission line behaves in a range of scenarios in terms of the energy propagation on the line and radiation from the line. Such approaches rely on 3D simulation tools which provide an accurate description of the structures but are very time consuming. However, the interest of a standard CISPR 25 setup to characterize a device under test (DUT) using equivalent dipoles has never been investigated. The interest of using such simple representative equivalent sources is twofold. First, no accurate knowledge about the devices under test is required. Second, these dipoles can be easily incorporated further in a 3D software to simulate the behaviour of the device in its real environment.

Both real source identification and far-field prediction are well-known problems in the electromagnetic compatibility (EMC) community. Different approaches can be found in the literature to find simplified and appropriate behavioral models of real embedded equipment.

Source identification consists in finding, with an inverse method, equivalent sources that radiate the same electromagnetic field as the measured one. In [9], both electric and magnetic dipoles, as equivalent sources, are determined by a genetic algorithm (GA) based optimization. In the literature, source identification is mainly achieved by magnetic near-field scanning measurements above PCBs (Print Circuits Boards) [10–14]. However, cartographies obtained by scanning measurements are sometimes composed of several hundreds of measurement points that greatly increase the calculation time of the inverse method. In [15], it was shown that a limited number of points with independent positions is sufficient to accurately predict the model source. For the case of one or two electric

* Corresponding author: Lionel Pichon (Lionel.Pichon@supelec.fr).

dipoles, ten measurement points are enough. However, to predict more complex sources accurately, a much higher number of points is needed since the inverse model is not linear to the variables. Equivalent dipoles can also represent apertures of an enclosure [16], antennas [17], integrated circuits [18, 19], or power electronic devices [20]. More recently, source identification was also applied in the time domain. In [21, 22], it was shown, for a transient signal having a wide frequency range, that a time domain analysis based on the time reversal method can overcome frequency domain limitations.

For far-field prediction, another method than using equivalent dipoles is based on Huygens surface [23]. In [24], an unclosed Huygens surface is proposed for predicting emissions below 30 MHz in a CISPR 25 test setup. The electric field distribution on the defined Huygens surface and the equivalent currents are estimated from a small number of near electric field measurements. The difference of the final predicted electric field at a 1 m distance (corresponding to the location of the rod antenna in the CISPR 25 test setup) is within 4 dB compared with a full-wave simulation. For frequencies above 30 MHz, a method based on a current scan and a multiple-dipole radiation model is proposed in [25].

This paper investigates the ability to reconstruct an equivalent radiation model directly from antenna measurements obtained with a CISPR 25 test setup. It describes a general modeling approach relying on antenna measurements in order to build a simplified but representative EMC model of a tested equipment. The reconstruction methodology is then developed to determine a set of equivalent dipoles of real electromagnetic sources. In Section 2.1, the expressions of the fields radiated by elemental electric and magnetic dipoles are presented. The methodology to obtain equivalent dipoles is then described in Section 2.2. The latter is validated in Section 3.1 with a 3D numerical simulation in the case of a microstrip line. An experimental protocol based on the CISPR 25 setup is proposed in Section 3.2 and allows to assess the potential of the source reconstruction approach. Finally, some conclusions and perspectives are drawn in Section 4.

2. DIPOLE MODEL

2.1. Electromagnetic Fields Radiated by Elemental Dipoles

The expressions of fields radiated by both electric and magnetic elemental dipoles are well known and given by [26]. For an elemental electric dipole (E-dipole), centered at the origin and traversed by an electric current $I_0\vec{z}$ (Figure 1(a)), the fields are:

$$\begin{aligned} H_r &= H_\theta = E_\phi = 0 \\ H_\phi &= j\,\frac{kI_0 l\sin\theta}{4\pi r}\left[1+\frac{1}{jkr}\right]e^{-jkr} \\ E_r &= \eta\,\frac{I_0 l\cos\theta}{2\pi r^2}\left[1+\frac{1}{jkr}\right]e^{-jkr} \\ E_\theta &= j\eta\,\frac{kI_0 l\sin\theta}{4\pi r}\left[1+\frac{1}{jkr}-\frac{1}{(kr)^2}\right]e^{-jkr} \end{aligned} \tag{1}$$

with (r,θ,ϕ) being the spherical coordinates, k the wave number, η the free space impedance, and l the electric dipole length. The magnitude of the electric dipolar moment is expressed as $M_{elec} = I_0 l$.

For an elemental magnetic dipole (H-dipole), centered at the origin and traversed by an electric current $I_0\vec{\Phi}$ (Figure 1(b)), the fields are:

$$\begin{aligned} E_r &= E_\theta = H_\phi = 0 \\ H_r &= j\,\frac{ka^2 I_0\cos\theta}{4r^2}\left[1+\frac{1}{jkr}\right]e^{-jkr} \\ H_\theta &= -\frac{(ka)^2 I_0\sin\theta}{4r}\left[1+\frac{1}{jkr}-\frac{1}{(kr)^2}\right]e^{-jkr} \\ E_\phi &= \eta\,\frac{(ka)^2 I_0\sin\theta}{4r}\left[1+\frac{1}{jkr}\right]e^{-jkr} \end{aligned} \tag{2}$$

with a being the radius of the magnetic dipole. The magnitude of the magnetic dipolar moment is expressed as $M_{mag} = I_0\pi a^2$.

The configuration of the electric and magnetic dipoles, where (1) and (2) can be used, is described in Figure 1. Thus, to facilitate the optimization procedure and easily implement some geometrical transformations, for any dipole, a coordinate transformation in cartesian frame is needed. The electric and magnetic fields (X stands for E or H) are then calculated with (3) for any position of the dipole, drawn in Figure 2, with a dipolar moment $\mathbf{M} = (M_x, M_y, M_z)$.

$$X(r,\theta,\phi) = A_{rs}\,Rot'_\phi\,Rot'_\theta\,A_{sr}\,X(R,\theta_{rot},\phi_{rot}) \tag{3}$$

$$A_{rs} = \begin{pmatrix} \sin(\theta)\cos(\phi) & \sin(\theta)\sin(\phi) & \cos(\theta) \\ \cos(\theta)\cos(\phi) & \cos(\theta)\sin(\phi) & -\sin(\theta) \\ -\sin(\phi) & \cos(\phi) & 0 \end{pmatrix} \tag{4}$$

$$A_{sr} = \begin{pmatrix} \sin(\theta_{rot})\cos(\phi_{rot}) & \cos(\theta_{rot})\cos(\phi_{rot}) & -\sin(\phi_{rot}) \\ \sin(\theta_{rot})\sin(\phi_{rot}) & \cos(\theta_{rot})\sin(\phi_{rot}) & \cos(\phi_{rot}) \\ \cos(\theta_{rot}) & -\sin(\theta_{rot}) & 0 \end{pmatrix} \tag{5}$$

$$Rot_\phi = \begin{pmatrix} \cos(\phi_r) & \sin(\phi_r) & 0 \\ -\sin(\phi_r) & \cos(\phi_r) & 0 \\ 0 & 0 & 1 \end{pmatrix} \tag{6}$$

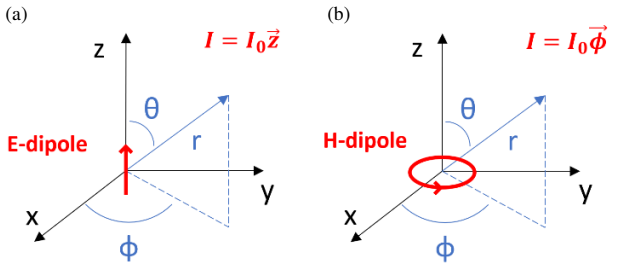

FIGURE 1. Configuration of elemental electric (a) and magnetic (b) dipole for using (1) and (2).

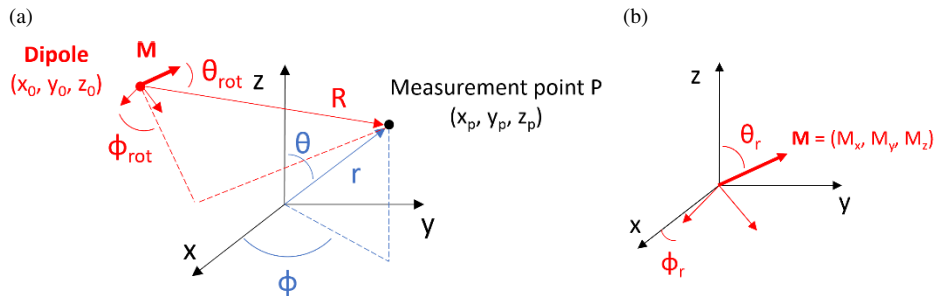

FIGURE 2. Configuration of elemental dipole for using (3) (a) and rotation angles for coordinate transformation (b).

$$Rot_\theta = \begin{pmatrix} \cos(\theta_r) & 0 & -\sin(\theta_r) \\ 0 & 1 & 0 \\ \sin(\theta_r) & 0 & \cos(\theta_r) \end{pmatrix} \tag{7}$$

$$\theta_r = \begin{cases} \pi/2 & \text{if } M_z = 0 \\ \pi - \text{atan}\left(\sqrt{M_x^2 + M_y^2}/-M_z\right) & \text{if } M_z < 0 \\ \text{atan}\left(\sqrt{M_x^2 + M_y^2}/M_z\right) & \text{if } M_z > 0 \end{cases} \tag{8}$$

$$\phi_r = \begin{cases} 0 & \text{if } M_x = 0 \,\&\, M_y = 0 \\ \pi/2 & \text{if } M_x = 0 \,\&\, M_y > 0 \\ -\pi/2 & \text{if } M_x = 0 \,\&\, M_y < 0 \\ \text{atan2}\,(M_y, M_x) & \text{if } M_x \neq 0 \end{cases} \tag{9}$$

with $X(R, \theta_{rot}, \phi_{rot})$ being the field calculated with (1) or (2) by using spherical coordinates $(R, \theta_{rot}, \phi_{rot})$ and the dipolar moment $|\mathbf{M}|$ (Figure 2), A_{rs} and A_{sr} the transformation matrix for rectangular-to-spherical and spherical-to-rectangular components, respectively, and Rot_ϕ and Rot_θ the rotation matrix regarding ϕ_r and θ_r, respectively.

For a measurement point $P = (x_p, y_p, z_p)$ and a dipole in position (x_0, y_0, z_0), the distance R is defined as:

$$\begin{cases} x_p = r\sin(\theta)\cos(\phi) \\ y_p = r\sin(\theta)\sin(\phi) \\ z_p = r\cos(\theta) \end{cases} \tag{10}$$

$$\begin{pmatrix} x_{rot} \\ y_{rot} \\ z_{rot} \end{pmatrix} = Rot_\theta Rot_\phi \begin{pmatrix} x_p - x_0 \\ y_p - y_0 \\ z_p - z_0 \end{pmatrix} \tag{11}$$

$$R = \sqrt{x_{rot}^2 + y_{rot}^2 + z_{rot}^2} \tag{12}$$

θ_{rot} and ϕ_{rot} are defined as θ_r and ϕ_r, respectively, but with conditions on $(x_{rot}, y_{rot}, z_{rot})$ instead of (M_x, M_y, M_z).

In CISPR 25, the Device Under Test (DUT) is above an elevated ground plane. Ground plane can be easily integrated into the model by using image theory [9, 13, 26]. The electromagnetic field emitted by a dipole above a ground plane at height h can be represented by two dipoles: the actual one and a fictitious one, the image of the actual one with respect to the ground plane (Figure 3).

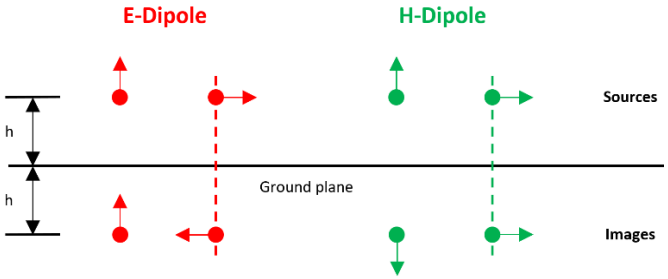

FIGURE 3. Images of electric and magnetic dipoles.

2.2. Description of the Methodology

The method considers that a source of radiation can be accurately substituted by a set of N equivalent dipoles. Therefore, the proposed methodology consists in measuring the magnitude of electric or magnetic field over a circle of radius r in three planes (XY, XZ, YZ) around the radiating structure, as indicated in Figure 4. Compared to the cartography approach observed in the literature, the proposed method uses a limited number of measurement points, reducing the computation time. Also, relying only on the magnitude of the field (without the phase consideration) was already proved to be an efficient reconstruction approach for the frequency range under study [10–12].

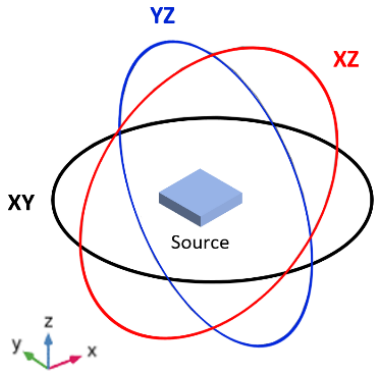

FIGURE 4. The three planes where the field is measured.

The positions $(x_{0,i},\ y_{0,i},\ z_{0,i})$ and dipolar moments $(M_{x,i},\ M_{y,i},\ M_{z,i})$ of the N equivalent dipoles are determined with an inverse method by using an optimization process based on a genetic algorithm (GA) followed by a pattern search (PS) method [11]. The first algorithm (genetic algorithm) is used for a global minimum search while the second (pattern search)

algorithm is used for a local search. Outputs of GA are inputs of PS. It was observed that such a hybrid optimization is better than only GA in terms of accuracy and computation time. This hybrid approach was proved to be suitable for various and complex field distributions in previous works. Equivalent sets of dipoles were deduced from the knowledge of the field distribution in the case of perforated walls [27], apertures in shielded enclosures [16], and emissions from power printed circuit boards [11]. The optimization function (OF) is defined as:

$$OF = \sqrt{\frac{\sum_{i=XY,XZ,YZ} \sum_{N_m} \left(E_{meas,i} - E_{mod,i}\right)^2}{3 \times N_m}} \quad (13)$$

with E_{meas} and E_{mod} being the measured and predicted electric fields from the N equivalent dipoles, respectively, and N_m the number of measurement points on one plane. In this paper, the study is only focused on the electric field norm, but the proposed method can also be used with electric field components and magnetic fields.

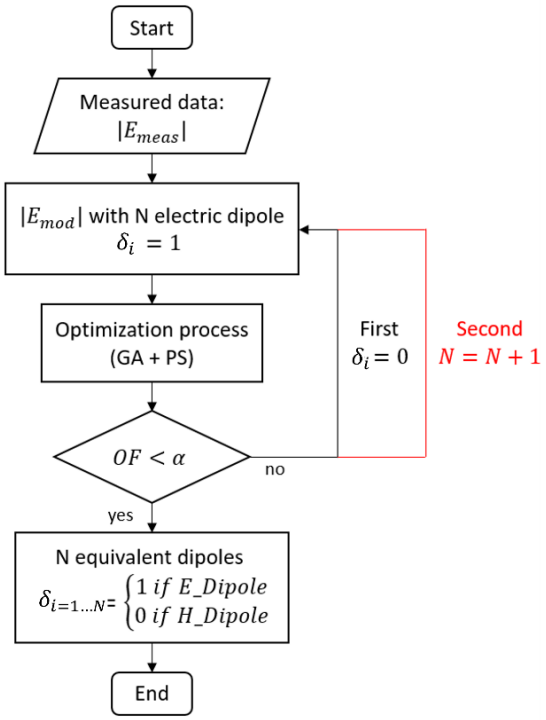

FIGURE 5. Flowchart of the proposed method.

The steps of the methodology are described in Figure 5. For each dipole, there are 7 parameters to determine: position ($x_{0,i}$, $y_{0,i}$, $z_{0,i}$), dipolar moments ($M_{x,i}$, $M_{y,i}$, $M_{z,i}$), and type δ_i, either electric ($\delta = 1$) or magnetic dipole ($\delta = 0$). Thus, the proposed algorithm firstly calculates the OF for an array of electric dipoles. If the prescribed error α is not reached, the dipole changes automatically to a magnetic one. For example, for two equivalent dipoles, the algorithm calculates the OF for two electric dipoles, then for one electric and one magnetic dipole, and finally for two magnetic dipoles. If after each case, the error is still not attained, it is advised to increase the number of equivalent dipoles. The algorithm can be obviously adapted to calculate the OF for a specific array of dipoles by putting a high error.

3. RESULTS AND VALIDATION

3.1. Numerical Validation

At first, the proposed model is validated with a numerical modelling of a simple radiating source. A microstrip line is modeled using COMSOL Multiphysics with the radio frequency (RF) module. The dimensions of the microstrip line are presented in Figure 6.

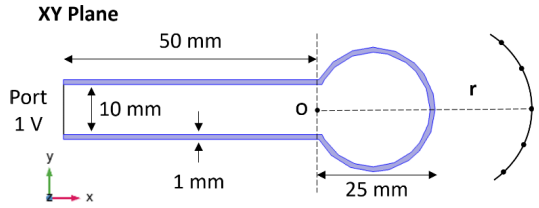

FIGURE 6. Dimensions of the microstrip line constituted of two arms and one loop.

The studied microstrip line is constituted of two arms with a length of 50 mm and a loop with a diameter of 25 mm. The distance between the two arms is 10 mm. The width of the conducting line is 1 mm. The microstrip line is excited at the end of the arms by a lumped port of 1 V. The computation is performed at 30 MHz. The electric field norm is measured around the microstrip line over a circle of radius r defined in the three planes (XY, XZ, YZ), as shown in Figure 4. For the inverse method, only 10 equidistant points on each circle are considered. Then, in this case, a total of 30 points are used to determine the equivalent dipoles. The equivalent dipoles are calculated at three measurement distances: $r_1 = 15$ cm, $r_2 = 25$ cm, and $r_3 = 50$ cm. As the microstrip line is a plane (no thickness), the positions z_0 of the dipoles are considered equal to 0. The parameters of the obtained dipoles are summarized in Table 1. The electric field radiated by the microstrip line is accurately reproduced by two equivalent dipoles, one electric and one magnetic, for the three studied distances. The electric fields of both microstrip line and equivalent dipoles are plotted in Figure 7 and Figure 8 respectively for the distances r_1 and r_3.

The E-H equivalent dipoles determined at the three distances are pretty similar in terms of positions and dipolar moments. Only a slight increase of the position x_0 is observed for both E and H dipoles. Both dipoles are between the two arms and close to the x-axis ($y_0 \approx 0$). The electric dipole and magnetic dipole are mainly oriented following the y-axis and z-axis, respectively. At distance r_1, three equivalent dipoles (E-E-H) have slightly better accuracy than the E-H equivalent dipoles by obtaining a smaller value of OF. It indicates that closer to the microstrip line, the electric field is more complex, and more dipoles are needed to accurately describe it. It can also be noted that the electric field at r_3 is reproduced relatively correctly with an H dipole only, as illustrated in Figure 8. It indicates that at this distance and farther, especially in the far

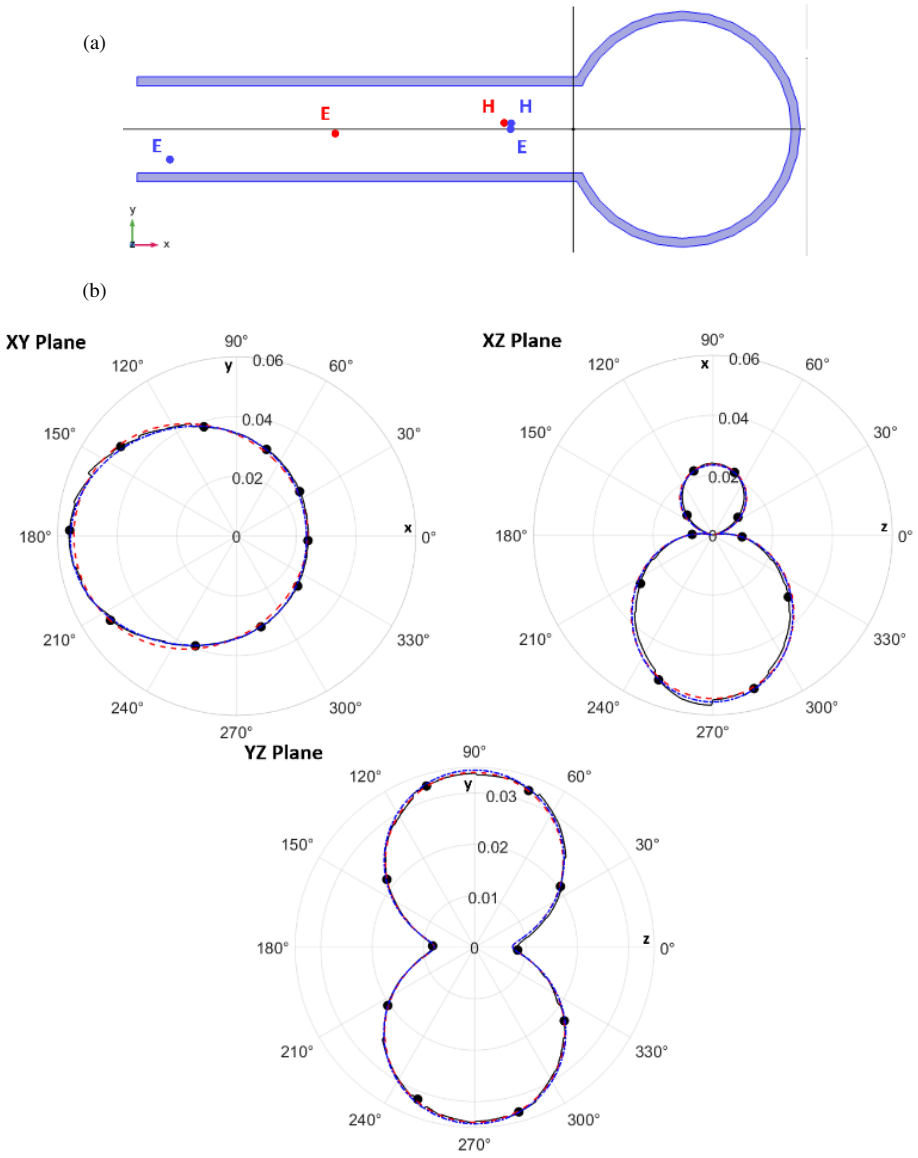

FIGURE 7. Positions of the E-E-H and E-H equivalent dipoles determined at r_1 (a), and electric field norm (V/m) over each plane radiated by the microstrip line (dark solid line), the E-H dipoles (red dashed line), and the E-E-H dipoles (blue dash-dotted line) (b). The dots indicate the measurement points considered in the inverse method.

TABLE 1. Parameters of the equivalent dipoles calculated at different distances.

Distance	OF V/m	Type of dipole	x_0, y_0, z_0 (mm)	M_x (A·m or A·m^2)	M_y (A·m or A·m^2)	M_z (A·m or A·m^2)
$r_1 = 15$ cm	6.5e-4	E	**−7.2**, 0.02, 0	−4.5e-8	**3.8e-7**	−3.1e-8
		E	**−46.2**, −3.5, 0	2.9e-8	**3.1e-7**	1.7e-8
		H	−7.1, 0.7, 0	−3.8e-7	6.3e-7	**3.9e-5**
	8.8e-4	E	**−27.3**, 0.5, 0	−1.5e-8	**7.0e-7**	−6.4e-9
		H	−7.9, 0.6, 0	−2.8e-7	1.0e-7	**3.9e-5**
$r_2 = 25$ cm	1.1e-4	E	**−26.1**, 0.7, 0	−1.0e-8	**7.0e-7**	1.2e-8
		H	−7.0, 0.5, 0	−2.3e-7	−4.3e-8	**3.9e-5**
$r_3 = 50$ cm	7.1e-6	E	**−25.0**, 0.03, 0	−7.0e-9	**6.9e-7**	3.5e-8
		H	−6.8, 0.08, 0	−2.3e-7	−1.6e-7	**3.9e-5**
	1.1e-4	H only	−31, −1.6, 0	−1.2e-6	−6.5e-7	**3.9e-5**

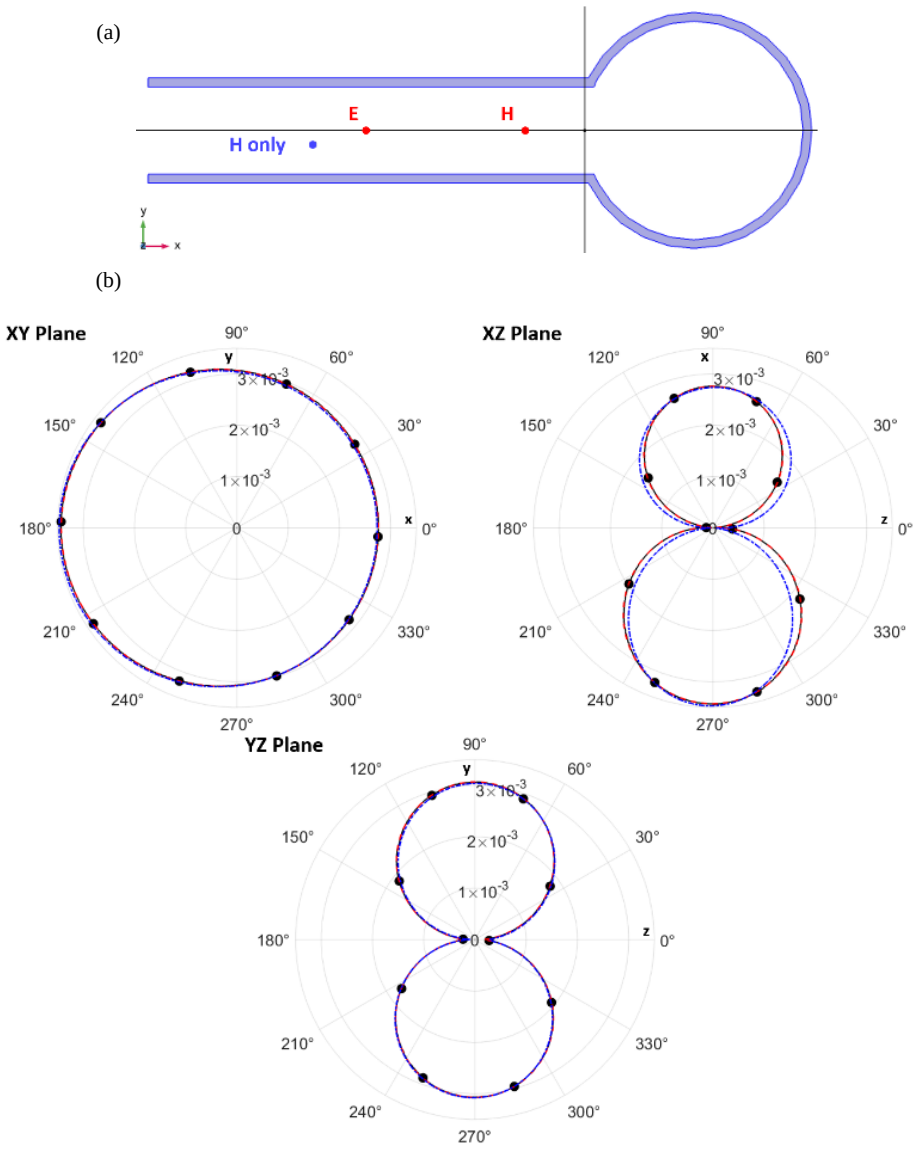

FIGURE 8. Positions of the E-H equivalent dipoles and H only dipole determined at r_3 (a), and electric field norm (V/m) over each plane radiated by the microstrip line (dark solid line), the E-H dipoles (red dashed line), and the H only dipole (blue dash-dotted line) (b). The dots indicate the measurement points considered in the inverse method.

field, the microstrip line can be assimilated to a single magnetic dipole.

Hence, even similar, the parameters of the obtained equivalent dipoles depend on the distance r_i at which they are evaluated, especially the number of equivalent dipoles. To estimate the accuracy of the electric field radiated by the E-E-H and E-H equivalent dipoles at other distances r, the median relative error is plotted in Figure 9. Globally, for distance $r \geq 25$ cm, the errors are under 3%. The lowest errors are obtained with the E-H dipoles determined at r_3 for distance $r \geq 35$ cm. The errors are higher for $r = 10$ cm, closer to the microstrip line, where the electric field is more complex. The lowest errors obtained at this distance are obtained with the E-E-H equivalent dipoles determined at r_1. Finally, a set of dipoles evaluated close to the radiating source is more suitable to estimate the field at other distances than a set of dipoles evaluated farther. Indeed, the E-H equivalent dipoles evaluated at r_3 show higher errors in the XZ plane (with minimal error at $r = r_3$) and greatly increase by reducing the distance r. To illustrate this point, the electric fields in the XZ plane radiated by the E-E-H equivalent dipoles evaluated at r_1 and the E-H equivalent dipoles evaluated at r_3 are plotted at 10 cm and 70 cm in Figure 10.

3.2. Experimental Protocol

To verify the validity of the proposed method, an experimental protocol is presented with a 30 cm monopole antenna as an emitting source. The setup, compliant with the CISPR 25 standard, places the DUT on an elevated ground. The electric field is measured with a 1 m rod antenna, and its counterpoise is often placed at the same height as the elevated ground. However, this configuration can lack reproducibility, introduce resonances,

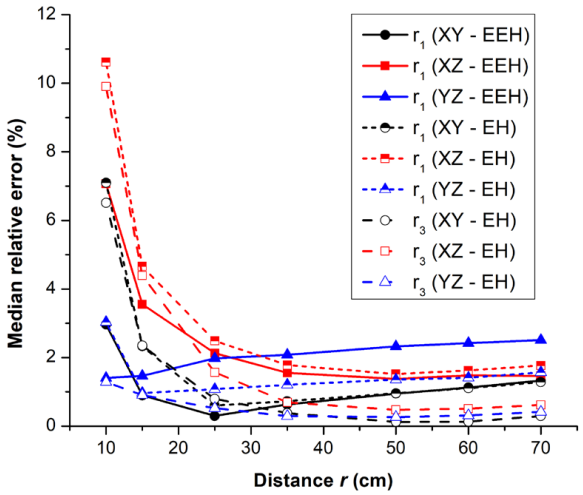

FIGURE 9. Median relative error between the electric field radiated by the microstrip line and the equivalent dipoles at different distance r for the E-E-H dipoles determined at r_1, the E-H dipoles determined at r_1 and r_3.

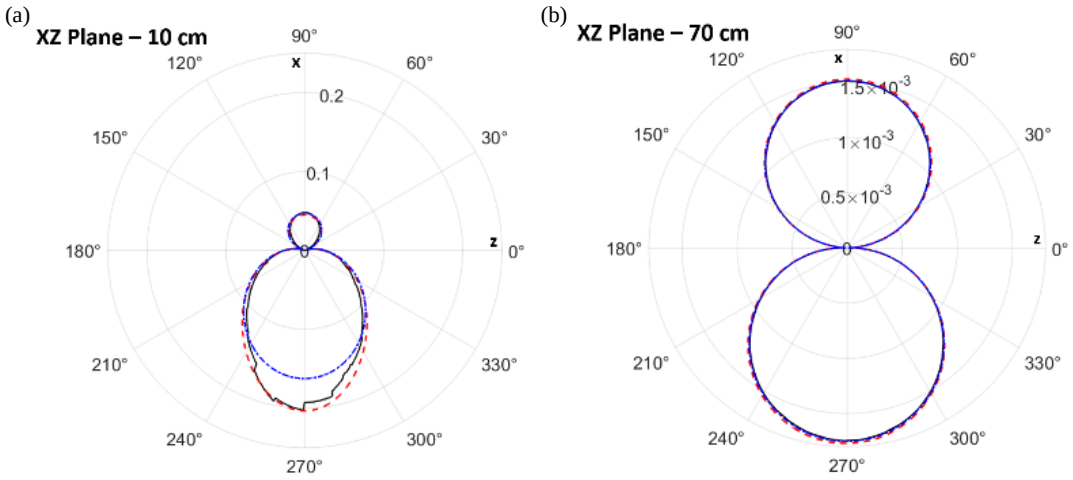

FIGURE 10. Electric field norm (V/m) in the XZ plane at $r = 10$ cm (a) and $r = 70$ cm (b) radiated by the microstrip line (dark solid line), the E-E-H equivalent dipoles evaluated at $r_1 = 15$ cm (red dashed line), and the E-H equivalent dipoles evaluated at $r_3 = 50$ cm (blue dash-dotted line).

and the electric field radiated by the source can be perturbed by the measuring system [28, 29]. Moreover, the electric field is diffracted by the edge of the elevated ground, due to its finite dimension. As previously mentioned, the ground can be introduced into the model thanks to the image theory; however, in this case, the ground is considered infinite. Thus, the diffraction effect can be difficult to consider, even if it seems possible to represent it by elemental dipoles [13, 30]. For all these reasons, both the emitting monopole antenna and receiving rod antenna are placed on the ground floor of a semi-anechoic chamber, as illustrated in Figure 11. The two antennas are placed at a one-meter distance. The monopole antenna is elevated by 15 cm with polystyrene blocks to get measurements above the noise level.

Measuring the electric field on the three planes is experimentally not feasible with the rod antenna. Instead, the measurement is performed with different orientations of the monopole antenna. For each orientation, the electric field is measured at five angles: $-70°$, $-35°$, $0°$, $35°$, and $70°$. To obtain the 10 points needed for the inverse method, the measurements are considered symmetric for the orientation XY (Figure 11(a)) and XZ (Figure 11(b)). For the orientation YZ (Figure 11(c)), two series of measurements are performed: one with the antenna facing the rod antenna (YZ front) and one with the antenna at the opposite (YZ rear). The electric field measurements at 100 kHz and 1 MHz for the four different orientations are presented in Figure 12 and Figure 13, respectively. The inverse method is used to determine the equivalent dipoles of the monopole antenna. As expected, the monopole antenna behaves similarly to a unique electric dipole. However, the field radiated by this E dipole does not perfectly describe the field of the monopole antenna. Increasing the number of dipoles does not rid this difference. However, a better solution is obtained by reducing the height z_d of the antenna base considered in the model from 15 cm to 7 cm. The same observations were also done at other frequencies.

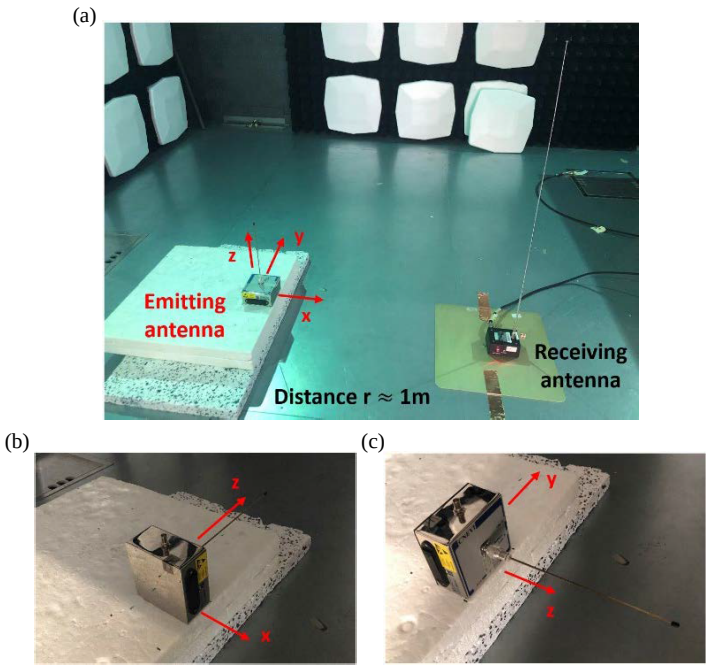

FIGURE 11. Experimental setup with different orientations of the monopole antenna: XY (a), XZ (b), and YZ (c).

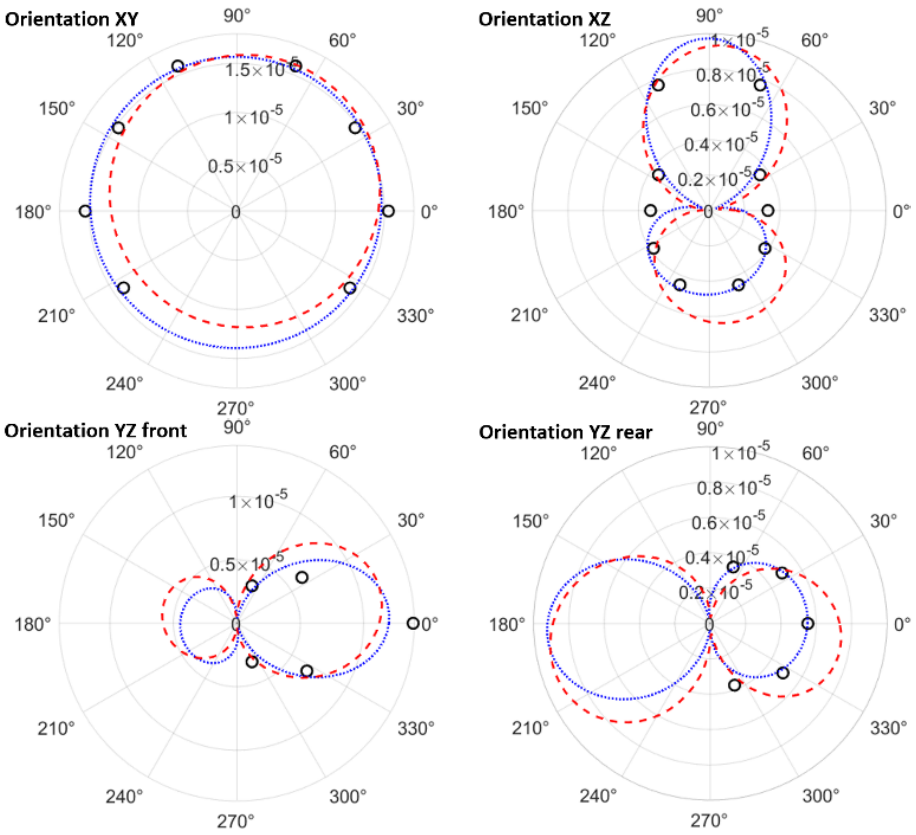

FIGURE 12. Electric field norm (V/m) for the four orientations of the monopole antenna measured at 100 kHz by the rod antenna (dark dot), and radiated by the equivalent electric dipole for $z_d = 15$ cm (red dashed line) and $z_d = 7$ cm (blue dotted line).

A major assumption could explain the fact that a better solution is obtained by not perfectly considering the experimental setup in the model. This assumption considers the rod antenna measurements as point measurements. Indeed, the antenna output voltage, and then the measured electric field based on it is not directly related to the electric field at a specific point in

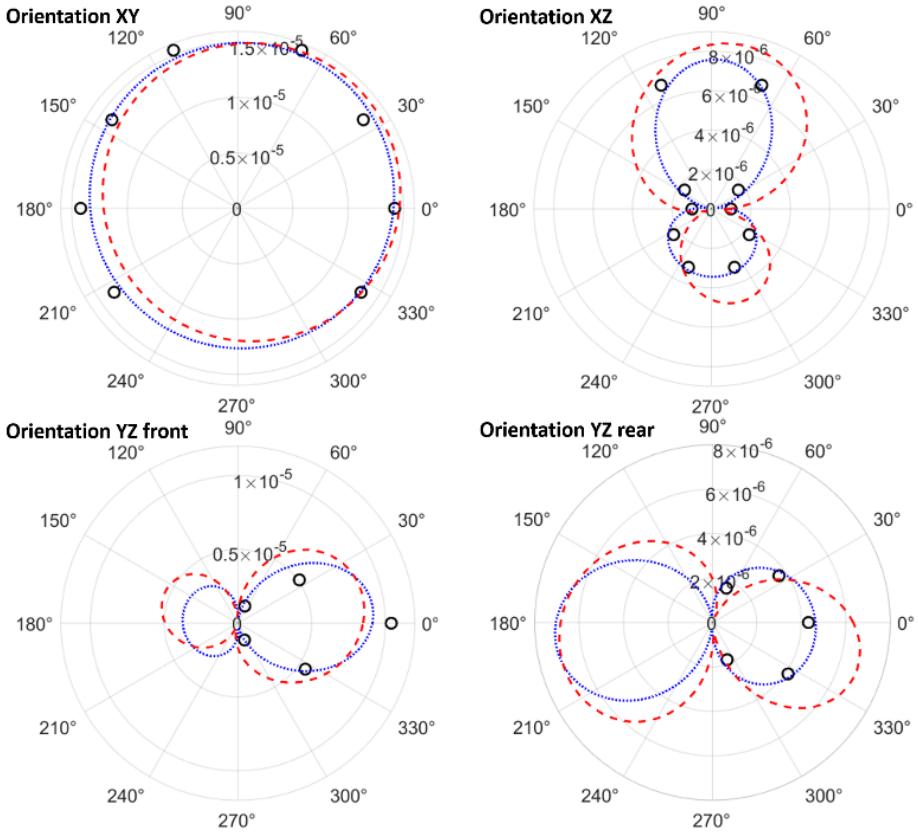

FIGURE 13. Electric field norm (V/m) for the four orientations of the monopole antenna measured at 1 MHz by the rod antenna (dark dot), and radiated by the equivalent electric dipole for $z_d = 15$ cm (red dashed line) and $z_d = 7$ cm (blue dotted line).

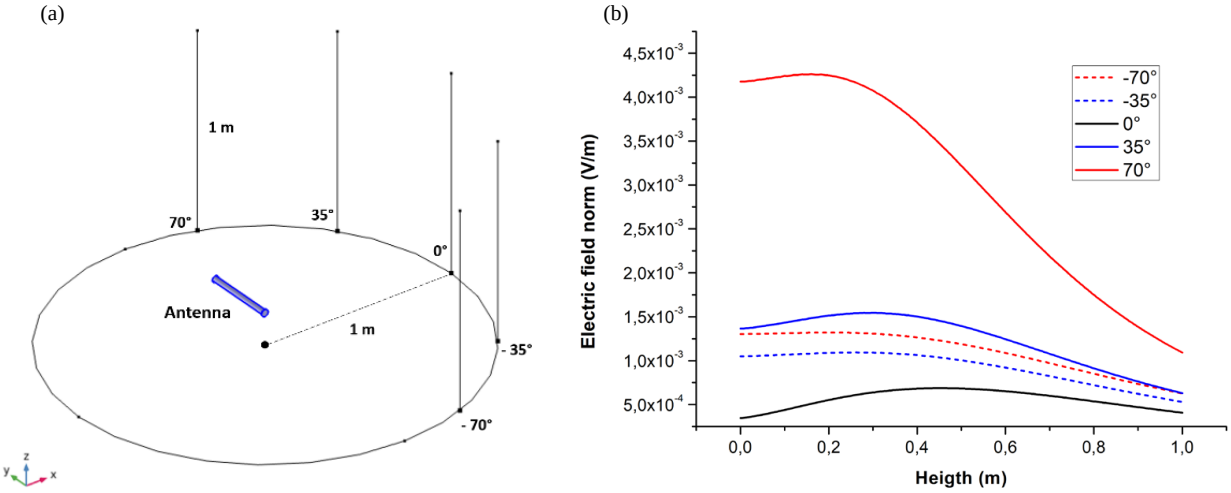

FIGURE 14. Geometry of the numerical model for the orientation XZ (a), and electric field norm (V/m) along the z-axis at the different angles at 1 MHz.

space, but it is rather proportional to its average along the antenna length [25]. Moreover, the rod antenna is immersed in a highly nonuniform electric field [28, 29]. To evaluate the impact of this assumption, a numerical model of the monopole antenna is developed. Only the emitting antenna rod is considered. The experimental geometry is respected, and the antenna base is placed 15 cm above a perfect electronic conductor ground (the antenna is 21 cm above). A lumped port of 1 V feeds the antenna. Moreover, like experimentally, the electric field is measured at 1 MHz for the four orientations of the antenna at a distance of 1 m at five angles, with point measurements distributed along the z-axis. The case of the orientation XZ is presented in Figure 14. The electric field along the z-axis slightly increases and then shows an important decrease, especially at the angle of 70°. The same behavior is observed at the other orientations. Thus, a higher heterogeneity is ob-

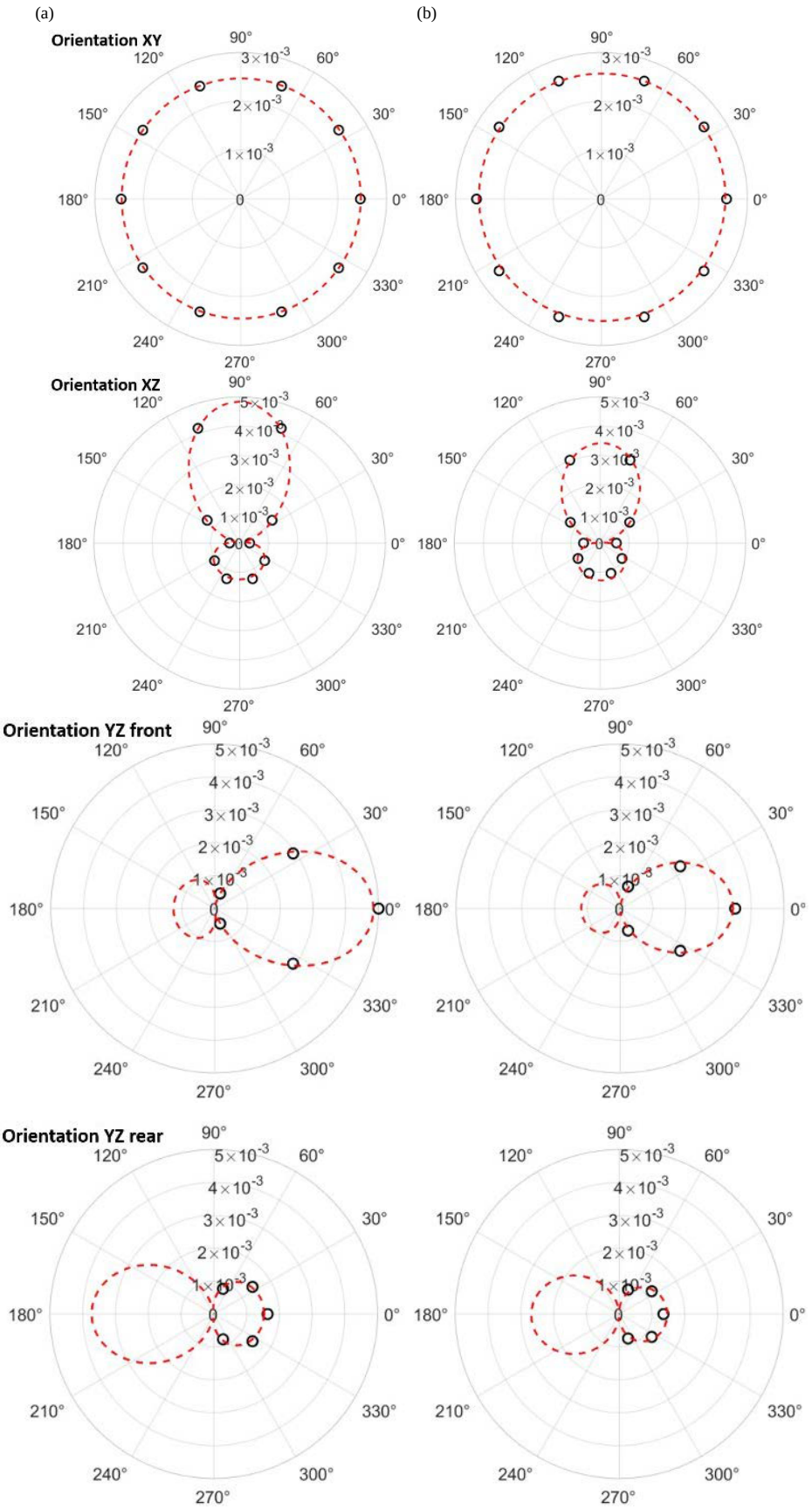

FIGURE 15. Electric field norm (V/m) at 1 MHz for the four orientations radiated by the antenna (dark dot) and its equivalent electric dipole (red dashed line) obtained with single point (a) and averaged values (b).

TABLE 2. Parameters of the equivalent dipoles calculated with single point and averaged electric field.

Type of value	Dipole	x_0, y_0, z_0 (mm)	M_x (10^{-6} A·m)	M_y (10^{-6} A·m)	M_z (10^{-6} A·m)
Single point	E	$-3.3, -1.9,$ **280**	1.2e-2	8.7e-3	**1.42**
Average (1 m)	E	11.2, 4.1, **231**	-2.6e-2	5.4e-3	**1.27**
Average (20 m)	E	$-2.5, -2.7,$ **279**	4.7e-3	1.1e-2	**1.45**

served when the antenna faces the measuring point. Now, the average values of the electric field norm along the z-axis over 1 m are considered in the methodology and compared to the single point values (plotted in Fig. 14).

The parameters of the equivalent electric dipole for both cases are summarized in Table 2. The norm of the electric field radiated by the antenna and the electric dipole is plotted in Figure 15 for the four orientations. Using the average electric field slightly increases the value in the orientation XY, from 2.46 mV to 2.57 mV. The smallest values in the other orientations also slightly increase, for example from 0.34 mV to 0.56 mV for the angle 0° in the orientation XZ. All other values decrease, and the greatest decrease is observed for the angle 0° in the orientation YZ front, from 5 mV to 3.5 mV. Thus, the equivalent electric dipole obtained by using the average value is not the same as the one obtained from a single-point value. It is slightly decentered along the x-axis, and its position z_0 and dipolar moment M_z are smaller. It was observed experimentally that reducing the height z_d of the antenna base considered in the model allows obtaining a more centered electric dipole. It is also the case here; a better-centered dipole is obtained with $z_d = 13.2$ cm instead of 15 cm. The experimental difference ($z_d = 7$ cm instead of 15 cm) is higher than the numerical one, especially due to additional error sources brought upon by experimental conditions. Moreover, it can be noted that using the averaged values over 20 cm, while the electric field is still not too heterogeneous, allows obtaining an electric dipole close to the ones obtained from single-point values (Table 2).

4. CONCLUSION

This paper has presented a source identification approach from antenna measurements to determine equivalent dipoles representative for an emitting electromagnetic equipment. The interest of the approach is to rely on a small number of antenna measurements. The approach is based on an inverse method using the magnitude of electric or magnetic field radiated by both elemental electric and magnetic dipoles. The electric field is measured along a circle in three orthogonal planes. A hybrid optimization method (GA + PS) is used to determine the parameters of the equivalent dipoles. The technique is first validated with a 3D full-wave simulation of a microstrip line. The electric field radiated in this case is accurately represented by only one electric and one magnetic dipole. However, closer to the microstrip line, three equivalent dipoles (E-E-H) are needed, and farther away, only a magnetic dipole can be enough. The equivalent dipoles determined close to the microstrip line (15 cm) can accurately predict the electric field radiated at other distances.

Then, an experimental protocol involving the test setup of the CISPR 25 standard is proposed by using a monopole antenna as the equipment under test. As expected, the behavior of this monopole antenna is similar to that of an electric dipole. However, using a 1 m rod antenna as the measurement sensor induces difficulties to recover the equivalent model with accuracy. Indeed, the rod antenna cannot be considered as a single-point measurement particularly due to the heterogeneity of the field along its length. This point has been verified with a 3D numerical simulation. The resulting compact model provides the radiated electric field with sufficient accuracy for several EMC analyses in the automotive industry. It allows to obtain the order of magnitude of the radiated electric field without the need to use near-field sensors (like electro-optical probes). In a challenging industrial context, a fast and low-cost approach can be decisive during the design stages. The provided compact and simple model of an equipment under test from standard measurements can be of crucial interest. The next step consists in evaluating how increasing the number of antenna measurements and/or taking some averaged values of the fields may reduce the errors on the results.

REFERENCES

[1] Yao, J., S. Wang, and Z. Luo, "Modeling, analysis, and reduction of radiated EMI due to the voltage across input and output cables in an automotive non-isolated power converter," *IEEE Transactions on Power Electronics*, Vol. 37, No. 5, 5455–5465, 2022.

[2] Pliakostathis, K., "Research on EMI from modern electric vehicles and their recharging systems," in *2020 International Symposium on Electromagnetic Compatibility (EMC Europe)*, 1–6, Rome, Italy, Sep. 2020.

[3] Zhang, Y., J. Guo, H. Liu, X. Zhang, Y. Wang, and Y. Fan, "EMI measurement and reduction for SiC MOSFET based motor drivers of electric vehicles," in *2023 3rd International Conference on Electrical Engineering and Mechatronics Technology (ICEEMT)*, 282–286, Nanjing, China, Jul. 2023.

[4] Yao, C.-Y. and W.-J. Liao, "An estimation method for EMI radiated emissions using measured source voltages," *IEEE Transactions on Electromagnetic Compatibility*, Vol. 65, No. 3, 770–779, Jun. 2023.

[5] Maouloud, A., M. Klingler, and P. Besnier, "A test setup to assess the impact of EMI produced by on-board electronics on the quality of radio reception in vehicles," *IEEE Transactions on Electromagnetic Compatibility*, Vol. 63, No. 6, 1844–1855, May 2021.

[6] IEC, "CISPR 25 — Vehicles, boats and internal combustion engines — Radio disturbance characteristics — Limits and methods of measurement for the protection of on-board receivers," 2021.

[7] Muniganti, H., B. Nayak, and D. Gope, "Diagnosis of radiating elements for CISPR 25 RE test setup using Huygens box method," *IEEE Letters on Electromagnetic Compatibility Practice and Applications*, Vol. 2, No. 2, 40–45, Jun. 2020.

[8] Sajjad, C. U., J. F. Dawson, A. Gunsaya, and A. Marvin, "Comparison of emissions from a transmission line on a CISPR 25 bench setup and test vehicle," in *2022 International Symposium on Electromagnetic Compatibility (EMC Europe)*, 90–95, Gothenburg, Sweden, Sep. 2022.

[9] Regue, J.-R., M. Ribo, J.-M. Garrell, and A. Martin, "A genetic algorithm based method for source identification and far-field radiated emissions prediction from near-field measurements for PCB characterization," *IEEE Transactions on Electromagnetic Compatibility*, Vol. 43, No. 4, 520–530, Nov. 2001.

[10] Liu, B., L. Beghou, L. Pichon, and F. Costa, "Adaptive genetic algorithm based source identification with near-field scanning method," *Progress In Electromagnetics Research B*, Vol. 9, 215–230, 2008.

[11] Benyoubi, F., L. Pichon, M. Bensetti, Y. L. Bihan, and M. Feliachi, "An efficient method for modeling the magnetic field emissions of power electronic equipment from magnetic near field measurements," *IEEE Transactions on Electromagnetic Compatibility*, Vol. 59, No. 2, 609–617, Apr. 2017.

[12] Zhao, W.-J., E.-X. Liu, B. Wang, S.-P. Gao, and C. E. Png, "Differential evolutionary optimization of an equivalent dipole model for electromagnetic emission analysis," *IEEE Transactions on Electromagnetic Compatibility*, Vol. 60, No. 6, 1635–1639, Feb. 2018.

[13] Thomas, D. W. P., C. Obiekezie, and X. Tong, "Equivalent dipole models of electromagnetic emissions from near-field scanning," *IEEE Electromagnetic Compatibility Magazine*, Vol. 4, No. 3, 74–78, Nov. 2015.

[14] Vives-Gilabert, Y., C. Arcambal, A. Louis, F. de Daran, P. Eudeline, and B. Mazari, "Modeling magnetic radiations of electronic circuits using near-field scanning method," *IEEE Transactions on Electromagnetic Compatibility*, Vol. 49, No. 2, 391–400, May 2007.

[15] Baklezos, A. T., C. D. Nikolopoulos, and C. N. Capsalis, "An equivalent dipole method with novel measurement positioning for modeling electric emissions in space missions," *Electromagnetics*, Vol. 37, No. 7, 439–453, Sep. 2017.

[16] Abdelli, W., A. Frikha, X. Mininger, L. Pichon, and H. Trabelsi, "Prediction of radiation from shielding enclosures using equivalent 3-D high-frequency models," *IEEE Transactions on Magnetics*, Vol. 51, No. 3, 7001504, Mar. 2015.

[17] Sijher, T. and A. Kishk, "Antenna modeling by infinitesimal dipoles using genetic algorithms," *Progress In Electromagnetics Research*, Vol. 52, 225–254, 2004.

[18] Ramesan, R. and D. Madathil, "Modeling of radiation source using an equivalent dipole moment model," *Progress In Electromagnetics Research B*, Vol. 89, 157–175, 2020.

[19] Xiang, F.-P., X.-C. Wei, and E.-P. Li, "A hybrid domain decomposition and optimization method for predicting electromagnetic emissions from printed circuit boards," *Journal of Electromagnetic Waves and Applications*, Vol. 29, No. 8, 1082–1092, 2015.

[20] Labiedh, W. and J. B. H. Slama, "Contribution of the PSO in the electromagnetic inverse method in terms of convergence and simplicity of implementation," *Journal of Electromagnetic Waves and Applications*, Vol. 28, No. 18, 2339–2349, 2014.

[21] Hedia, S., B. Zitouna, J. B. H. Slama, and L. Pichon, "Electromagnetic time reversal in the near field: Characterization of transient disturbances in power electronics," *IEEE Transactions on Electromagnetic Compatibility*, Vol. 62, No. 5, 1869–1878, Oct. 2020.

[22] Hedia, S., B. Zitouna, J. B. H. Slama, and L. Pichon, "Time domain sources identification in the near field: Comparison between electromagnetic time reversal and genetic algorithms-based methods," *IET Science, Measurement & Technology*, Vol. 14, No. 10, 842–847, Dec. 2020.

[23] Pan, J., X. Gao, and J. Fan, "Far-field prediction by only magnetic near fields on a simplified Huygens's surface," *IEEE Transactions on Electromagnetic Compatibility*, Vol. 57, No. 4, 693–701, Aug. 2015.

[24] Chen, Z. and S. Frei, "A near-field measurement based method for predicting field emissions below 30 MHz in a CISPR-25 test set-up," *Advances in Radio Science*, Vol. 14, 147–154, Sep. 2016.

[25] Jia, J., D. Rinas, and S. Frei, "Predicting the radiated emissions of automotive systems according to CISPR 25 using current scan methods," *IEEE Transactions on Electromagnetic Compatibility*, Vol. 58, No. 2, 409–418, Apr. 2016.

[26] Balanis, C. A., *Antenna Theory: Analysis and Design*, 2nd ed., John Wiley & Sons, New York, 2016.

[27] Briki, I., L. Pichon, and J. B. H. Slama, "Shielding effectiveness of perforated screens through an inverse problem-based resolution," *IEEE Transactions on Magnetics*, Vol. 52, No. 3, 8000604, Mar. 2016.

[28] Gandolfo, A., R. Azaro, and D. Festa, "Improving the accuracy of radiated emission measurements for frequency below 30 MHz by using a fiber optic isolated rod antenna," in *2017 IEEE International Symposium on Electromagnetic Compatibility & Signal/Power Integrity (EMCSI)*, 63–68, Washington, DC, USA, Aug. 2017.

[29] Carobbi, C., "Resonance free operation of the rod antenna for 1 m distance testing up to 30 MHz," in *2019 IEEE International Symposium on Electromagnetic Compatibility, Signal & Power Integrity (EMC+SIPI)*, 554–559, New Orleans, LA, USA, Jul. 2019.

[30] Obiekezie, C., D. W. P. Thomas, A. Nothofer, S. Greedy, L. R. Arnaut, and P. Sewell, "Optimisation of a simple equivalent dipole model to include edge effects," in *2013 International Conference on Electromagnetics in Advanced Applications (ICEAA)*, 672–675, Turin, Italy, Sep. 2013.